

TOOLS AND TECHNIQUES

Patterns of organelle ontogeny through a cell cycle revealed by whole-cell reconstructions using 3D electron microscopy

Louise Hughes¹, Samantha Borrett¹, Katie Towers¹, Tobias Starborg² and Sue Vaughan^{1,*}**ABSTRACT**

The major mammalian bloodstream form of the African sleeping sickness parasite *Trypanosoma brucei* multiplies rapidly, and it is important to understand how these cells divide. Organelle inheritance involves complex spatiotemporal re-arrangements to ensure correct distribution to daughter cells. Here, serial block face scanning electron microscopy (SBF-SEM) was used to reconstruct whole individual cells at different stages of the cell cycle to give an unprecedented temporal, spatial and quantitative view of organelle division, inheritance and abscission in a eukaryotic cell. Extensive mitochondrial branching occurred only along the ventral surface of the parasite, but the mitochondria returned to a tubular form during cytokinesis. Fission of the mitochondrion occurred within the cytoplasmic bridge during the final stage of cell division, correlating with cell abscission. The nuclei were located underneath each flagellum at mitosis and the mitotic spindle was located along the ventral surface, further demonstrating the asymmetric arrangement of cell cleavage in trypanosomes. Finally, measurements demonstrated that multiple Golgi bodies were accurately positioned along the flagellum attachment zone, suggesting a mechanism for determining the location of Golgi bodies along each flagellum during the cell cycle.

KEY WORDS: Organelle inheritance, SBF-SEM, Glycosome, Acidocalcisome, Flagellum, Kinetoplast, Golgi body, Mitochondrion, Abscission

INTRODUCTION

Morphogenesis of cell shape and polarity is a key feature of cell division, and in unicellular organisms this is particularly well orchestrated. This often allows the identification of cells at various stages of cell division by morphology alone due to asymmetrical morphogenesis, which results in two identical daughter cells. For instance, in *Saccharomyces cerevisiae* a small bud forms, which increases in size during cell division and post cytokinesis; organelles are actively transported from the mother to the smaller budding daughter cell in an ordered manner via the actin cytoskeleton (Knoblauch and Rachubinski, 2015a). The mother cell must retain a portion of organelles and this is achieved via connections to the cell periphery involving both the cytoskeleton and endoplasmic reticulum (Knoblauch and Rachubinski, 2015b; Oh and Bi, 2011; Pollard and Wu, 2010). This type of asymmetry


during cell division may have been important in the evolution of eukaryotic cell differentiation.

One of the major challenges to studying complex spatiotemporal changes through the cell division cycle has been in visualizing organelles and cellular structures in a three-dimensional (3D) context. Confocal microscopy has been an invaluable tool in recent years, but requires cellular structures to be labelled with a fluorophore, so usually only one or two different epitopes can be visualized in a single cell. Cellular electron tomography has allowed high-resolution 3D imaging of ultrastructure within a limited area of a cell, but it is not feasible to reliably produce large numbers of whole individual cells. Serial block face scanning electron microscopy (SBF-SEM) is a relatively new technique that uses a backscattered electron detector and a modified ultramicrotome inside an SEM chamber to sequentially slice and image the surface of a sample embedded in a resin block (Denk and Horstmann, 2004). Hundreds of images can be collected, producing large datasets that can be segmented by various 3D software packages (Denk and Horstmann, 2004; Hughes et al., 2014). Owing to well-documented changes in cellular shape and organelle duplication in the protozoan parasite *T. brucei* through the cell cycle (Robinson et al., 1995; Sherwin and Gull, 1989; Wheeler et al., 2013), a sequential order of the cell cycle progression can be determined for individual whole cells, and this work represents the first detailed quantitative and spatiotemporal analysis of cells through the cell division cycle by 3D reconstructions at an ultrastructural level.

The general architecture of the *T. brucei* cell is a long slender shape, which is maintained by a corset of subpellicular microtubules at the cell cortex. This highly ordered and stable set of microtubules cover the entire surface of the body and are cross-linked to each other (Hemphill et al., 1991; Sherwin and Gull, 1989; Vickerman, 1969a). The single flagellum is attached along the long axis of the cell and is attached to the cell body via the flagellum attachment zone (FAZ) (Sherwin and Gull, 1989; Vaughan, 2010; Vickerman, 1969a,b). During the cell division cycle, the basic cell shape is maintained and the microtubule cytoskeleton remains intact. The flagellum also remains intact and the new flagellum grows alongside it. As the new flagellum grows, it moves to a posterior position relative to the old flagellum, leading to one daughter cell forming posterior to the other. The division fold bisects the cell asymmetrically between the two flagella, but leads to two approximately identical cells (Wheeler et al., 2013), but the new flagellum continues to grow after cytokinesis (Farr and Gull, 2009). Clearly, organelles must also be organized along asymmetrical lines to ensure correct inheritance when cytokinesis occurs. Unlike many animal cells, a myosin II contractile ring does not form in *T. brucei* at the division fold (Farr and Gull, 2009; Hammarton et al., 2007; Wheeler et al., 2013). However, some significant structures and organelles (e.g. mitochondrial DNA contained within the kinetoplast, nucleus, Golgi body and endoplasmic reticulum) are positioned along the long axis of the cell in the region where the

¹Department of Biological and Medical Sciences, Faculty of Health and Life Science, Oxford Brookes University, Oxford OX3 0BP, UK. ²Wellcome Centre for Cell Matrix Research, University of Manchester, Michael Smith Building, Manchester M13 9PT, UK.

*Author for correspondence (svaughan@brookes.ac.uk)

 S.B., 0000-0003-4292-858X; K.T., 0000-0001-9187-8027; S.V., 0000-0002-0925-4491

flagellum is attached to the cell (He, 2007; Lacomble et al., 2012; Vaughan and Gull, 2008), suggesting that the FAZ is important for organelle inheritance in *T. brucei*.

In this study, we have used SBF-SEM to reconstruct whole individual cells at different stages of the cell cycle, giving an unprecedented and detailed analysis of the spatiotemporal changes to organelle positioning and copy number through the cell cycle at the ultrastructural level. We have defined a set of axes to enable comparison of different cell cycle stages as well as quantified whole cell volume measurements, organelle number and growth measurements for most organelles in the cell. This has highlighted a complex arrangement of organelles and revealed new spatiotemporal features of Golgi body position, mitochondrion biogenesis and mitotic spindle placement.

RESULTS

Stages of the cell cycle were determined using distinct ultrastructural features

Volumes containing up to 1000 sequential images (100 nm thick Z-slices) containing hundreds of individual bloodstream-form trypanosomes from an asynchronous population were collected by SBF-SEM. Segmentation (modelling) of whole cells was carried out using AMIRA software and the large volume cell organelles were

reconstructed. Many whole and partial cells (cells that had a portion of the cell body or flagella outside of the data volume) were analysed, and a total of 79 whole cells, containing all of the organelles and the full length of the flagella, were modelled in their entirety. The number of cells included in the analysis for each organelle is indicated in the figures. Fig. 1A (Movie 1) is a representative G1 cell illustrating the spatial organization of the organelles that were modelled. These include the flagellum (purple, attached to the cell body), cell body membrane (transparent yellow), basal bodies (white, positioned at the proximal end of the flagellum), Golgi bodies (green, located in the cell along seam where the flagellum is attached to the cell body), the nucleus (transparent blue) containing a nucleolus (blue), glycosomes (orange), acidocalcisomes (grey), and a mitochondrion (transparent green) with a kinetoplast (green, which contains the mitochondrial DNA and is physically attached to the basal bodies at the proximal end of the flagellum close to the flagellar pocket) (Ogbadoyi et al., 2003). The endoplasmic reticulum (ER) was reconstructed but has not been included in this analysis because the z-axis resolution, as determined by slice thickness, was too large for accurate modelling and quantification of the relatively thin ER sheets.

In order to compare the positioning and orientation of cellular components between cell cycle stages, a set of axes were defined. The dorsal surface of the cell (Fig. 1A,B, labelled D) was defined as

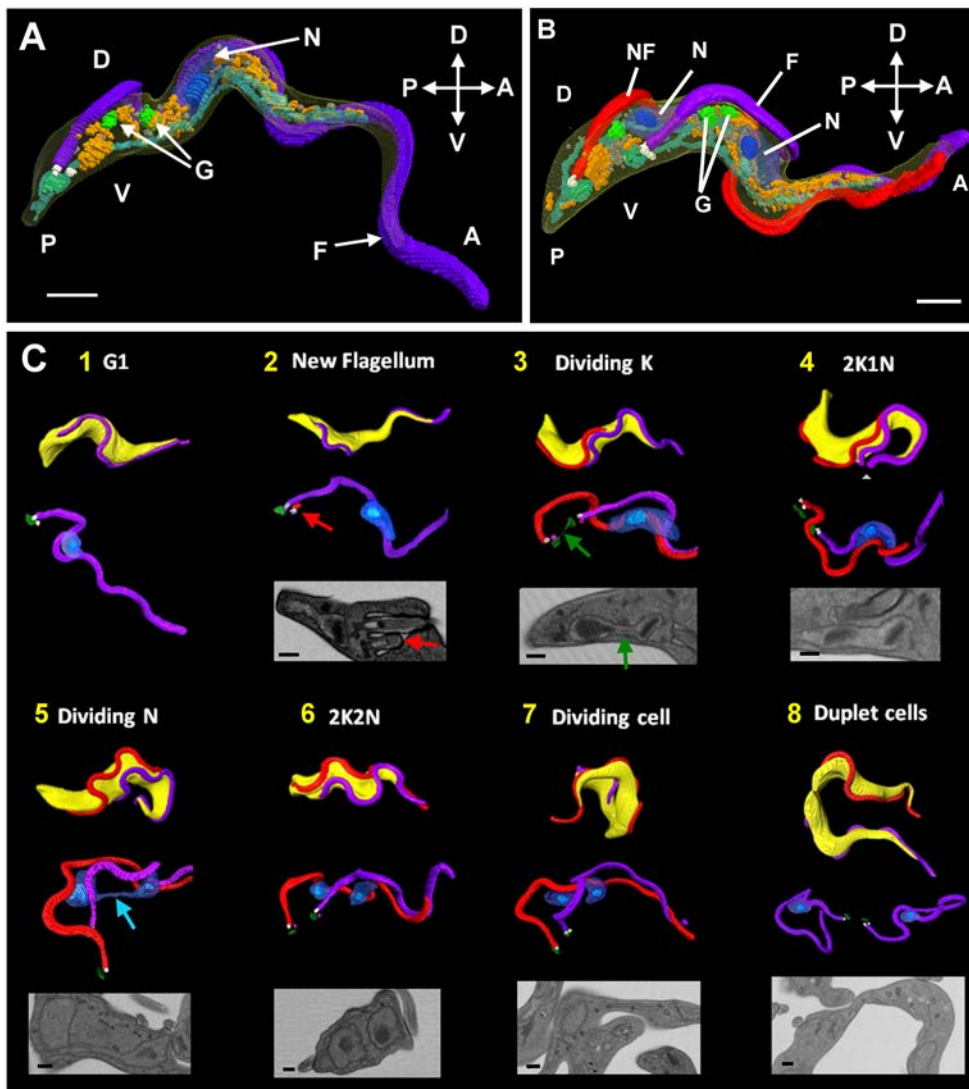


Fig. 1. Distinct ultrastructural features were used to determine cell cycle stages. (A) Surface rendering of a segmented G1 cell showing the spatial organization of organelles. (B) Surface rendering of a post mitotic cell containing two nuclei (N, transparent blue). Organelles are labelled and coloured as follows: the flagellum (F, purple), new flagellum (NF, red), Golgi body (G, green), mitochondrion (pale blue), glycosomes (orange), acidocalcisomes (grey), basal bodies (white) and nucleolus (dark blue). Cell orientation is indicated as follows: dorsal (D) and ventral (V); anterior (A) and posterior (P). (C) Surface renderings and SBF-SEM data showing the key ultrastructural features used to determine stage of cell cycle (stages 1–8). (1) Cell with single flagellum, nucleus and kinetoplast (dark green). (2) Cell with a new flagellum that has not exited the flagellar pocket (red arrow). (3) Cell with dividing kinetoplast with a nabelschnur (green arrow). (4) Cell with two separated kinetoplasts and no nabelschnur. (5) Mitotic cell with the two lobes of the nucleus linked by membrane that is placed along the ventral surface (blue arrow). (6) Two separate kinetoplasts, and nuclei and division fold forming. (7) Cells showing furrow ingression at the anterior end of the cell. (8) Daughter cells that have nearly completed furrow ingression and are only connected at their posterior ends (also called duplet cells). Scale bars: 1 μ m (A,B); 500 nm (C).

the surface where the flagellum is attached along the long axis of the cell body. The ventral surface was defined as opposite the dorsal surface (Fig. 1A,B; labelled V). The anterior end of the cell (Fig. 1A,B; labelled A) contains a portion of free flagellum and is the leading end for cell movement. The proximal end of the flagellum (purple) and basal bodies (white) are situated close to the posterior end of the cell (Fig. 1A,B; labelled P). Fig. 1B (Movie 2) illustrates a post-mitotic dividing cell with a new flagellum (red) which grows attached to the cell alongside the old flagellum. The new flagellum is always precisely positioned posterior and to the left of the old flagellum during its growth with the division fold and cleavage furrow bisecting the cell between the two flagella (Sherwin and Gull, 1989). The growth and precise positioning of the new flagellum allows whole cells to be ordered according to cell cycle progression (Sherwin and Gull, 1989; Tyler et al., 2001; Wheeler et al., 2013; Woodward and Gull, 1990). To observe changes in cell morphogenesis and organelle number through the cell cycle, cells were further divided into eight subsets using distinct and well-characterized ultrastructural features described below and summarized in Fig. 1C. The volume and number of individual organelles and cell structures were also assessed within these eight defined cell cycle stages and are described below and summarized in Tables S1 and S2.

Spatial organization and quantification through the cell cycle

Early cell cycle stages 1–4

Prior to entry into the cell cycle, the parasite contained a single flagellum, a pair of basal bodies, a single kinetoplast (containing the mitochondrial DNA, kDNA), nucleus, a single mitochondrion located along the ventral portion of the cell, either 1 (60%) or 2 (40%) Golgi bodies and an average of 62 glycosomes and 40 acidocalcisomes (see Fig. 1A,C1 and Tables S1, S2, which outlines all volume, number and/or length changes through the eight cell cycle stages). Stage 2 cells demonstrated the first stage of cell growth with the presence of a short new flagellum within the

flagellar pocket (Fig. 1C2; arrow), which coincides with S-phase (Sherwin and Gull, 1989). Analysis of cells prior to entering the cell cycle (stage 1; Fig. 1C1) and cells in stage 2 (Fig. 1C2) revealed that all measured organelles, except acidocalcisomes, significantly increased in volume or number after entry into the cell cycle ($P < 0.001$ for nucleus and cell body volume, $P < 0.01$ for kinetoplast volume and Golgi body number $P < 0.05$ for mitochondrion volume and glycosome number increasing to 75, $n = 6$ stage 2 and $n = 10$ for stage 1 cells) (Tables S1, S2; Figs 2–6).

Changes in the spatial organization of organelles through the cell cycle were also compared. During stages 3 and 4, cell body volume increased (Fig. 2A), new flagellum growth continued out of the flagellar pocket (Fig. 2B) and kDNA segregation occurred (Fig. 1C3,C4). The volume of the mitochondrial DNA density of the kinetoplast increased significantly at stage 2 when kinetoplast S-phase occurred, reaching a maximum in stage 3 (these measurements included the nabelschnur in stage 3) (Fig. 3). In addition, the Golgi bodies increased in number and were located at the flagellum attachment zone area (Fig. 4), as previously described (Bangs, 2011). Branching was observed in the mitochondrion along the ventral surface only (Fig. 1A, Fig. 5 and Movies 1, 4) and the nucleus elongated along the long axis of the cell (Fig. 3C2–C4,F). Trypanosomes undergo a closed mitosis with no breakdown of the nuclear membrane (Vickerman and Preston, 1970). The mammalian bloodstream cell is long and slender, and the diameter of the nucleus is only slightly smaller than the diameter of the thickest part of cell. An interesting question is how the nucleus increases in size under these constraints. Measurements confirmed that the nucleus elongated only along the long axis of the cell during stages 2–4 while the width did not change significantly (Fig. 3C1–C4,F; Tables S1, S2; Fig. 1). The mitochondrion was observed initially to branch only at the anterior end of the cell during stage 2 (Fig. 5A1–A4). Fenestrations and looped regions were observed towards the central and posterior end of the cell as the cell cycle progressed through stages 2–4. However, branching did not fill the cell body with mitochondrion, but instead spread out over the ventral region,

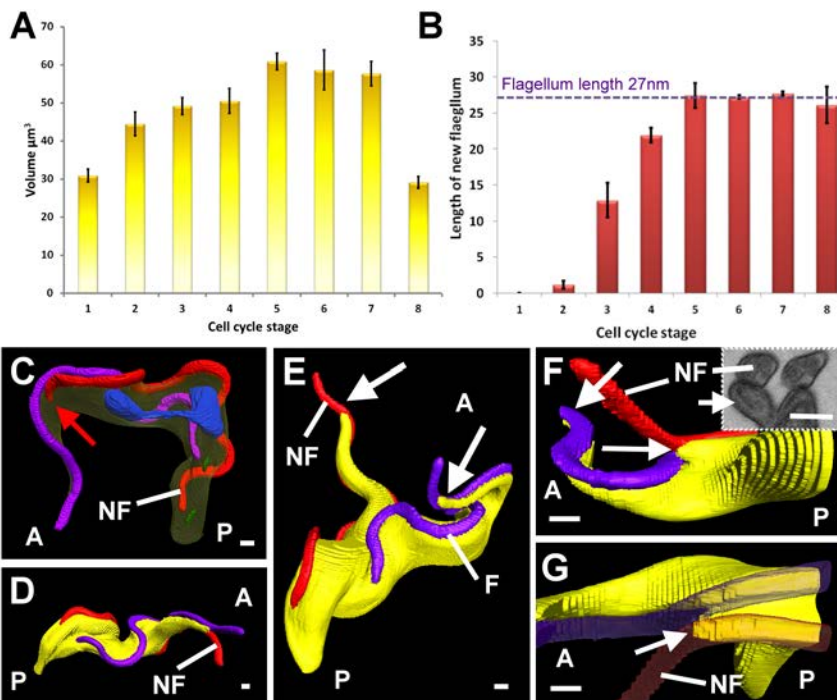


Fig. 2. Changes in cell volumes and flagella length occur during the cell cycle. (A) Changes in cell volume across the stages of the cell cycle as outlined in Fig. 1 (stages 1–8). Errors bars show the s.d.; $n = 43$. (B) Changes in the length of the new flagellum across the cell cycle. The mean normal flagellum length is 27 µm and is shown as a dashed line for comparison with the new flagellum length. Error bars are the standard deviation ($n = 3–4$ for each stage in the cell cycle, total $n = 25$). (C) Stage 5 cell showing that the tip of the new flagellum has not reached the anterior tip of the cell (arrow). (D) Stage 6 cell showing that the new flagellum (NF) extends out from the anterior end of the cell to the same degree as the old flagellum. (E) A stage 7 cell undergoing cytokinesis from the anterior end. F, old flagellum. (F, G) Surface rendering of data from the same cell to illustrate the formation of a new anterior cell tip for the new flagellum (NF) (G; arrow). Tip view (F) from the dorsal surface and (G) from the ventral surface. In C–G, anterior is denoted by A and posterior by P. Scale bars: ~500 nm.

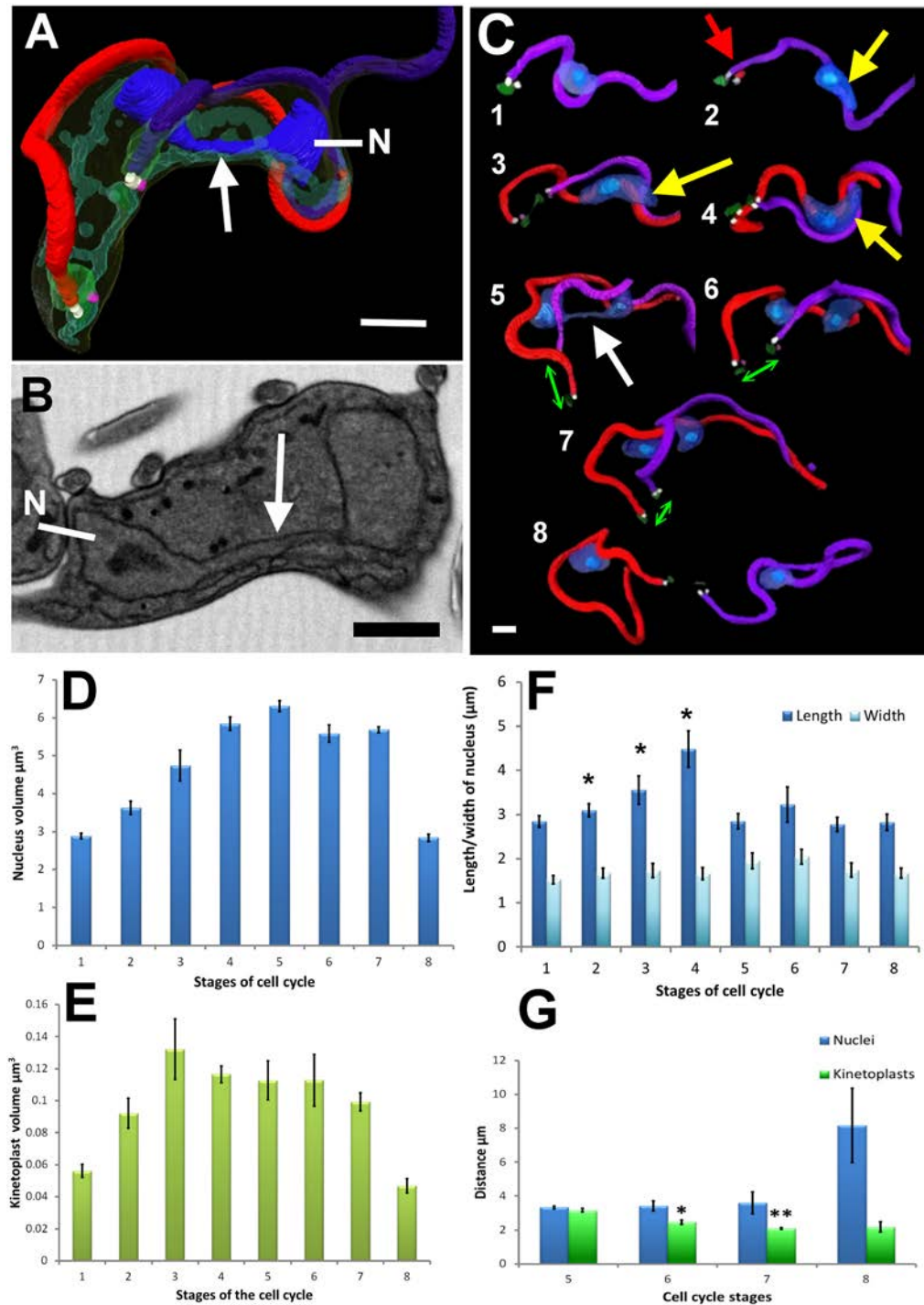


Fig. 3. The relative positions of kinetoplasts and nuclei change following segregation. (A) Surface rendering and (B) micrograph of SBF-SEM data showing a mitotic nucleus (N) with the connecting membrane (arrow) located in a ventral position within the cell. (C) Surface rendering of representative cells through the cell cycle (stages 1–8) showing changes in nucleus morphology (yellow arrows) and relative kinetoplast position (green arrows). The ventral position of the connecting membrane between the two nuclear lobes (white arrow) and the early formation of a new flagellum (red arrow) are also indicated. Scale bars: ~1 μm. (D) Nucleus and (E) kinetoplast volumes across the cell cycle (stages 1–8). In stage 3, the nabelschnur of the kinetoplast (Gluezn et al., 2011) was included in the measurements. (F) Length (blue) and width (light blue) of the nuclei (individual lobes of the mitotic nucleus) were measured for stage 5 across the cell cycle. * $P < 0.05$ (for the increase in the length of the nucleus observed between stages 1 and 2, 2 and 3 and 3 and 4). (G) The distance between pairs of kinetoplasts and nuclei from stage 4 onwards. * $P < 0.05$, ** $P < 0.01$ indicate a significant difference in the distance between kinetoplasts compared with stage 5 cells. There was no significant difference in the distance between nuclei at stages 5–7.

suggesting a mechanism to limit expansion into the mid and dorsal aspects of the cell (see below). Golgi bodies were identified by the presence of clear cisternae (Fig. 4A,B, arrows) and ~4–5 stacks were evident. All Golgi bodies were located beneath either the old or new flagellum within the cell body and closely aligned with the flagellum attachment zone (FAZ) along the long axis of the cell (Fig. 1A,B, Fig. 4A,B,C). As the cell cycle progressed through stages 2–4 there were between 2–4 Golgi bodies per cell (Fig. 4D).

Reconstructions of individual cells using SBF-SEM allowed, for the first time, an accurate counting of multi-copy organelles through the cell cycle. Metabolism of host glucose by glycolysis is the only source of ATP production in the bloodstream form of the parasite

and is partly carried out in a separate membrane-bound subcellular compartment called the glycosome. The tubular shaped glycosomes were often observed in clusters, and most glycosomes within a cluster exhibited the same orientation (Fig. 6A). Glycosomes either singularly or in clusters were found to be distributed throughout the cell body (Fig. 6A,C,F). Counts of glycosomes ($n=56$ cells) revealed that the average number in a stage 1 cell was 62, which compares well with previous work (Tetley and Vickerman, 1991). A significant increase in glycosome number was observed in stage 2 cells to 75 per cell ($P < 0.05$). The average glycosome number per μm^3 of cell body was 0.5 in a G1 cell and this was maintained as cell volume increased through the cell cycle (Fig. 6D). Energy

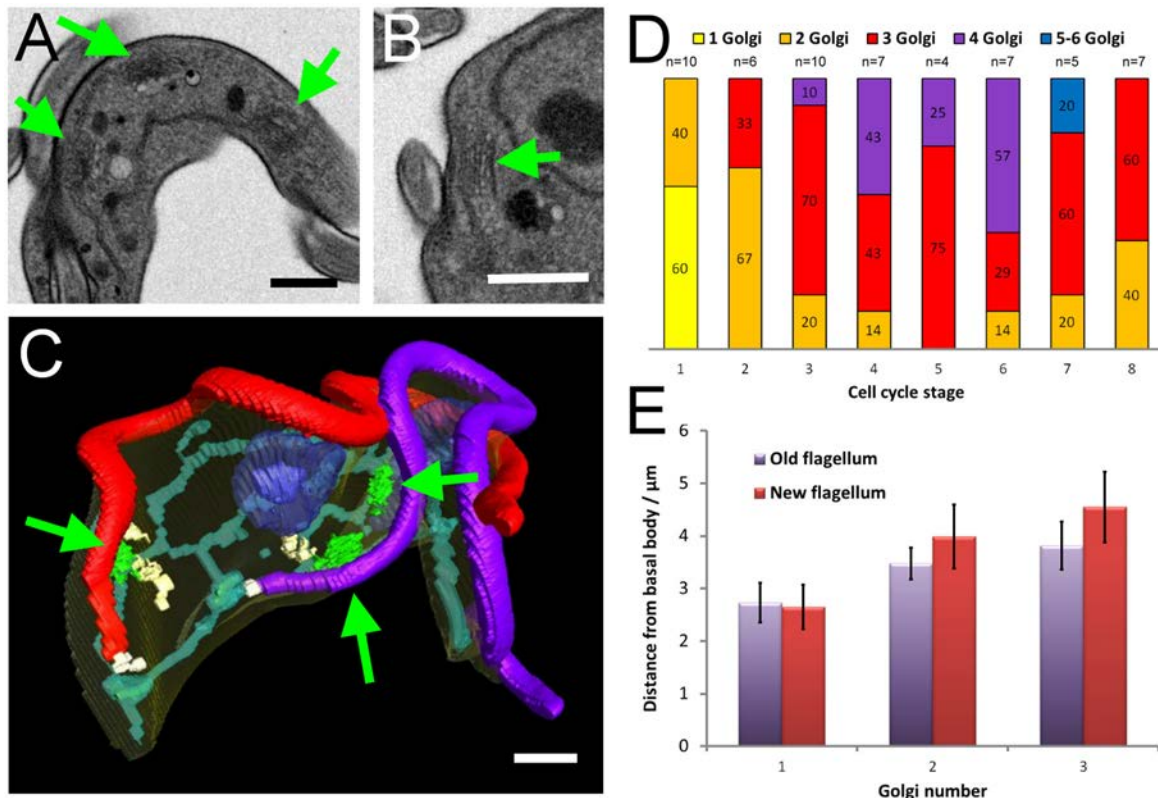


Fig. 4. The number of Golgi bodies per cell changes across the cell cycle. (A,B) Single micrographs from SBF-SEM data showing (A) three Golgi bodies (green arrows) lined up beneath a single flagellum and (B) close up of a single Golgi body showing the stacks and vesicles (green arrow). (C) Surface rendering of segmented data showing three Golgi bodies (green arrows) lining up beneath the flagella. (D) Percentage of cells with 1–6 Golgi bodies across stages of the cell cycle (stages 1–8). *n* values are indicated at the top for each stage of the cell cycle. (E) Distance from the basal body along the flagellum to each of the up to three Golgi bodies that were observed along each flagellum, numbered 1–3 posterior to anterior. No significant difference was observed between the old and new flagella. Error bars indicate standard deviation. *n*=36 (Golgi 1), 26 (Golgi 2) and 7 (Golgi 3). Scale bars: ~1 μm.

requirements would expect to increase as cells progressed through cell division and there was a positive correlation between cell body volume and glycosome number (correlation coefficient 0.876468) through the cell cycle. These data demonstrate that, at least in cultured bloodstream form cells, glycosomes increase as soon as the cell cycle starts and maintenance of glycosome number is probably important for energy requirements as the cell increases in size.

Acidocalcisomes are also a multicopy organelle in *T. brucei* and are Ca²⁺ storage organelles which were first identified in trypanosomes, but have been discovered in a wide range of eukaryotic organisms (Docampo and Huang, 2015; Vercesi et al., 1994). They have a distinctive ultrastructure in certain chemical fixation protocols making them easy to identify (Fig. 6B). Acidocalcisomes appeared to be evenly distributed from the flagellar pocket to the anterior end of the cell and throughout the cell body. The average number of acidocalcisomes in a stage 1 cell was 40 (*n*=56) (Fig. 6E). The number of acidocalcisomes did not increase significantly at early stages of the cell cycle (stages 2 and 3), suggesting there is not an immediate requirement as the cell increases in size.

Mitosis and cell abscission (stages 5–8)

Cells in mitosis were identified by the presence of two distinct lobes of the nucleus with membrane linking them. During mitosis, nucleus volume peaked in stage 5 cells (Fig. 1C5; Fig. 3A) and each lobe of the nucleus was positioned underneath one of the two flagella with the connecting membrane positioned towards the ventral surface of the cell (Fig. 3A,B; arrows). Spindle microtubules

were not visible within the membrane connection due to the resolution of the data. At this stage the cell possessed two segregated kinetoplasts located at the proximal end of each of the two flagella. Cell volume reached a maximum at mitosis of 61 μm³ (stage 5), twice the size of a G1 (stage 1) cell (Fig. 2A). There were between three and four Golgi bodies in total, distributed beneath the old and new flagella (Fig. 1B, Fig. 4C), and the mitochondrion branched across the ventral surface of the cell (Fig. 5; Movie 4). The 3D organization of organelles during mitosis shows a significant role for the flagella in the positioning of the Golgi bodies (Fig. 4C), kinetoplasts and nuclei (Fig. 3A) ready for cell cleavage, with the mitochondrion branching out across the opposing, ventral surface (Fig. 5A5; Movie 3). Glycosome number increased to average of 103 at mitosis and acidocalcisomes increased to 52 with no change in their distribution in the cell body (Fig. 6; Tables S1, S2).

Stage 6 was characterized by cells with two separate nuclei, each positioned underneath a flagellum, and a division fold present between the two flagella. This stage is where major cytoskeleton and shape changes occur as two daughter cells are formed (Wheeler et al., 2013). Measurements showed that cell volume was similar during stages 6 and 7, demonstrating that a further cell volume increase was not required for formation of the division fold or cleavage furrow. Glycosome (108) and acidocalcisome (56) number continued to increase as cell division progressed (Tables S1, S2). The formation of a new anterior end for the new flagellum daughter cells also formed at this stage, but how this occurs is poorly understood. The flagellum is attached along the cell body until the

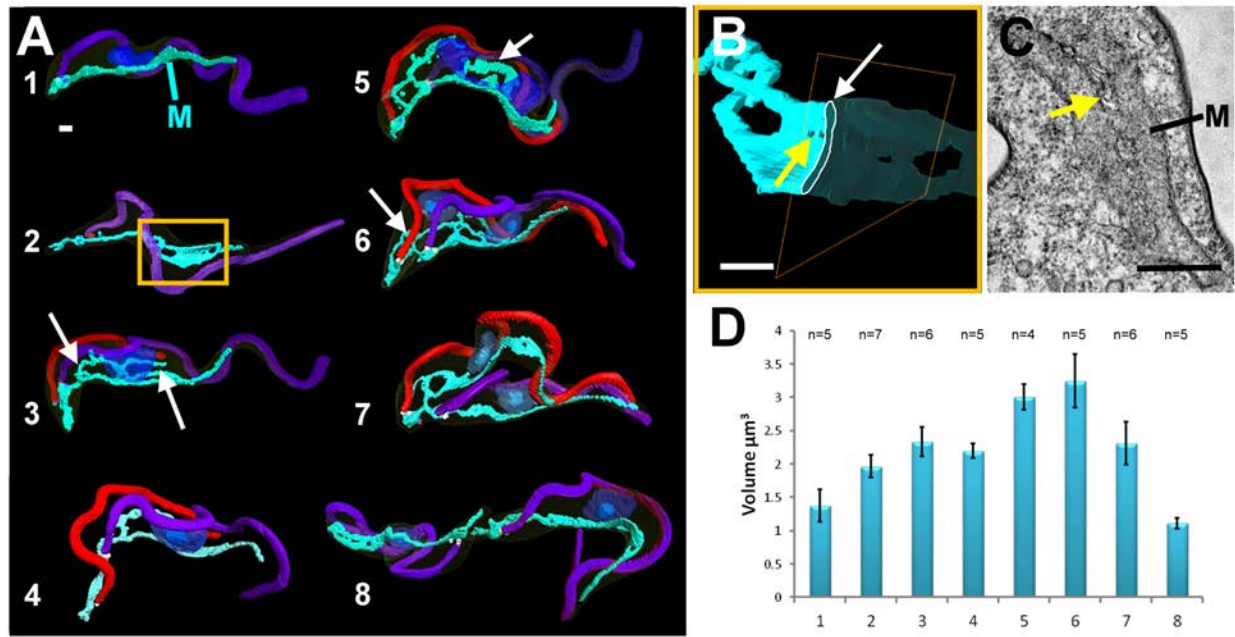


Fig. 5. Mitochondrial morphology changes during the cell cycle. (A) Surface rendering of segmented data showing changes in the mitochondrion (M) through the cell cycle (stages 1–8) from a single tube to interconnected loops (arrows). (B) Enlarged view of the boxed region in A with half the flattened region as a solid surface and half shown in transparency so that the flattened plate in cross section (white arrow) is revealed. Small holes or fenestrations can be observed in the flattened area (yellow arrow). (C) Transmission electron micrograph of a thick section (200 nm) showing the same flattened mitochondrial structure (M) with fenestrations (yellow arrow). (D) Changes in the mean mitochondrial volume across the cell cycle. Error bars indicate standard deviation and *n* values are listed at the top of the chart. Scale bars: ~500 nm.

anterior tip of the cell, where a portion of the flagellum extends forward and is unattached. An intriguing question is how and when a new anterior end forms for the new flagellum daughter cell. The

average length of the old flagellum was 27 µm (*n*=29) across all cell cycle stages and did not alter significantly at any point in the cell cycle (Fig. 2B, blue dotted line; Tables S1, S2). The distal tip of a

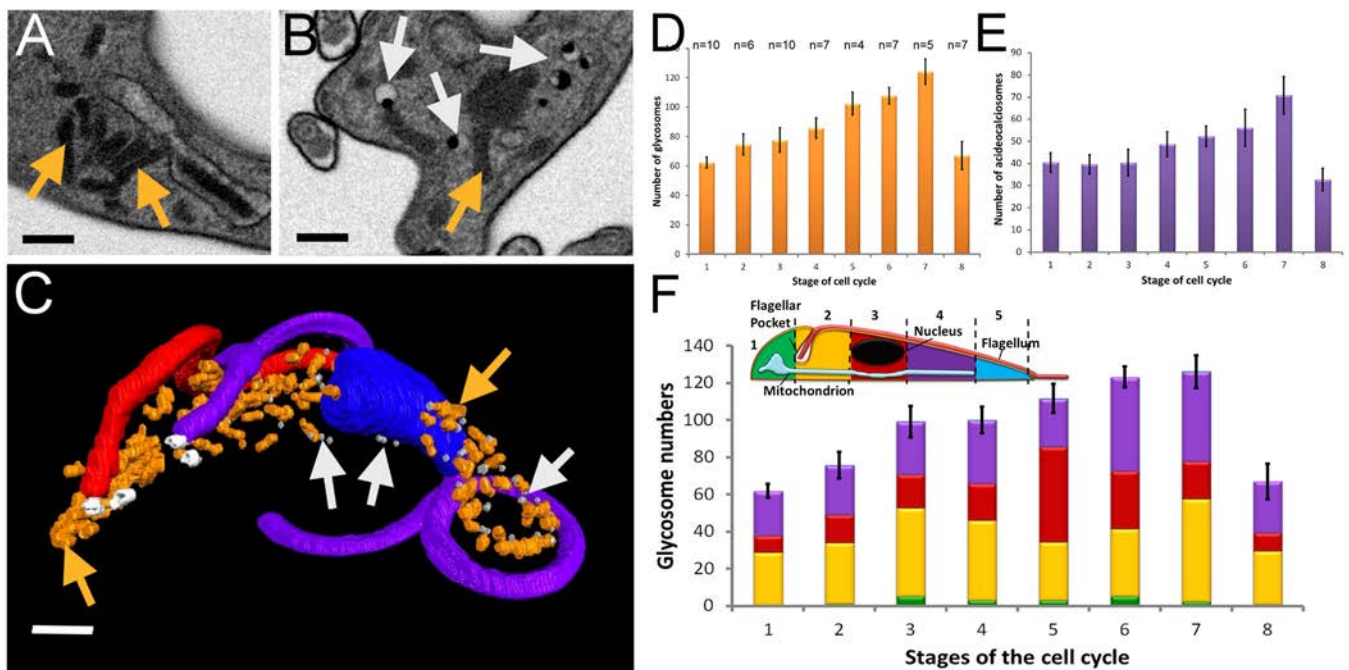


Fig. 6. Glycosomes and acidocalcisomes increase in number prior to cell division. (A,B) SBF-SEM micrographs and (C) a surface rendering of segmented data showing the ultrastructure and distribution of glycosomes (orange arrows) and acidocalcisomes (white arrows). Scale bars: ~500 nm. (D) The average number of glycosomes in a cell across the cell cycle (stages 1–8). *n* values are indicated for each stage in the cell cycle. (E) The average number of acidocalcisomes in a cell across the cell cycle. *n* values are the same as in D. (F) Distribution of glycosomes within a cell across the cell cycle (*n*=4 for all stages except 5 where *n*=3). The regions were posterior to the flagella pocket (green), between the posterior of the flagella pocket and the most posterior position of the nucleus or nuclei (yellow), between the posterior of the nucleus or nuclei and the anterior of the nucleus or nuclei (red), between the most anterior position of the nucleus or nuclei and the anterior of the mitochondrion (purple), anterior to the end of the mitochondrion (blue). Error bars indicate standard deviation.

growing new flagellum in bloodstream forms is located in a unique invagination of the cell body membrane, called the groove, until it reaches the anterior end of the cell (Hughes et al., 2013), and this groove must resolve in order for the new flagellum to extend beyond the end of cell. The distal tip of the new flagellum was still in the groove during mitosis (stage 5) (Fig. 2C, arrow) and had reached same length as the average for the old flagellum (Fig. 2B). By stage 6, when the division fold had formed, the distal tip of the new flagellum was no longer located in the groove but had extended out from the cell (Fig. 2D, labelled NF). The distal tip of the new flagellum extended to the same distance front of the anterior tip of the cell as the old flagellum (Fig. 2D). However, the length of unattached new flagellum averaged $3.9\ \mu\text{m}$ ($n=11$, stages 6–8) and was significantly ($P<0.001$) longer than for the old flagellum (average $2.7\ \mu\text{m}$, $n=21$, stages 1, 6–8). The detachment point of the new flagellum was not at the tip of the cell, as with the old flagellum, but was located $\sim 1\ \mu\text{m}$ behind it. We propose that this is the position at which the groove (Hughes et al., 2013) is resolved and that this coincides with where the anterior tip of the new cell was observed to form (Fig. 2F,G). Resolution of the flagellum groove and morphogenesis of anterior ends occurred during formation of the division fold.

A further morphogenetic event occurring during stage 6 was a reduction in the distance between the segregated kinetoplasts, noted previously using light microscopy (Tyler et al., 2001). It is well documented that kinetoplasts segregate prior to mitosis (Fig. 3G), but the distance between the two kinetoplasts significantly reduced between stages 5 to 6 when the division fold was forming and again between 6 and 7 during initiation of the cleavage furrow (Fig. 3G). The distance between the two nuclei did not change from stages 5–7 (Fig. 3G), although spatially the new nuclei appeared to have re-positioned alongside each other, rather than one located posterior to the other along the long axis (compare Fig. 3C5 and 3C7). This suggests an additional morphogenetic event in the two daughter cells that coincides with division fold formation when major changes are occurring in the subpellicular microtubule corset (Wheeler et al., 2013).

Cell cleavage occurred between flagella and along the division fold in stage 7 (Fig. 1C7) and the maximum number of glycosomes and acidocalcisomes was observed at this stage. Stage 8 cells (called duplet cells) were attached to each other via their posterior ends, just prior to abscission. For the purpose of comparison to G1 cells, and because the two daughter cells are distinct, each daughter of the duplet cells was analysed separately in the results presented throughout this paper (Fig. 1C8). At stage 8, the volume of each daughter cell had a similar volume to stage 1 cells. This demonstrates that in the bloodstream form of *T. brucei*, cell body volume only increases and decreases following initiation of the cell cycle and not during the G1 phase.

Extensive mitochondrial branching along the ventral surface through formation of mitochondrial fenestrations

Trypanosomes are an extreme example in eukaryotes in having just one mitochondrion that spans the length of the cell and have novel aspects that make the mitochondrion potentially important for discovery of novel drug targets (Verner et al., 2015). Accurate inheritance is crucial with just a single mitochondrion, but how tubular mitochondria are segregated and inherited is poorly understood within eukaryotic cells. In mammalian cells, inheritance of mitochondria is thought to be a passive process that occurs via fragmentation during mitosis ready for distributing to

daughter cells. Fragmentation of the mitochondrion has not been shown in *T. brucei* and genes for mitochondrial fusion have also not been identified in *T. brucei* (Esseiva et al., 2004).

No mitochondrial fragmentation was observed from reconstructions of mitochondria from all cell cycle stages. Instead, there is a highly organized mechanism for mitochondrial partitioning. In stage 1 cells (G1 cells) the single tubular mitochondrion was only located along the ventral surface of the cell body (volume $1.4\ \mu\text{m}^3$) (Fig. 1A, Fig. 5A1; Movie 1). During the cell cycle, areas of the mitochondrion in the anterior portion of the cell body exhibited an expansion into flattened thickened areas (Fig. 5A2, boxed, 5B arrow). Movie 3 illustrates one of these flattened areas. Small fenestrations were observed within these flattened regions (Fig. 5B,C, arrows), suggesting that the flattening of the membrane might be required for the production of fenestrations and subsequent larger loops of the connected mitochondrion. Despite the production of a branched mitochondrial network along the ventral surface, there remained one fully connected mitochondrion. As the cell cycle progressed through stages 2–4, further fenestrated mitochondrion was observed towards the central portion of the cell along with larger loops of mitochondrion, possibly as a result of the fenestrations fusing together (Fig. 5A3, arrowhead). Volume measurements revealed that the mitochondrion increased as the cell cycle progressed, from an average of $1.4\ \mu\text{m}^3$ in G1 cells to a maximum of $3.2\ \mu\text{m}^3$ post-mitosis (stage 6) (Fig. 5D; Tables S1, S2; $n=43$) when the division fold formed. An elaborate network of interconnected loops was formed along the ventral surface by the time the cell entered mitosis (stage 5) (Fig. 5A2–A5; Movie 4). A decrease in volume occurred in stage 7 cells, and the volume of the mitochondrion in each duplet cell in stage 8 was similar to the volume in G1 (stage 1) cells. Morphologically, following mitosis and during formation of the division fold and cleavage in stages 6 and 7, the mitochondrial network appeared to simplify. There was a reduction in flattened regions and loops resulting in the presence of the tubular mitochondrion once again, suggesting that fusion of the loops could be taking place (Fig. 5A6–A7). By stage 8 (Fig. 5A8), the mitochondrion was almost a single tube as in stage 1 cells and there was little evidence of flattened or looped regions. These results demonstrate a distinct polarity of mitochondrion biogenesis along the ventral surface of the cell body. Extensive branching does not persist once the division folds forms, indicating that branching along the ventral surface serves to place portions of the mitochondrion in the correct position prior to furrow ingression.

Mitochondrial fission occurs within the cytoplasmic bridge prior to cell abscission

A single tubular mitochondrion traversed each nascent daughter cell during furrow ingression in stage 7 cells (Fig. 5A8), and was present in the narrow opening between the two daughter cells even in stage 8 cells. In some cells, the tubular mitochondrion traversed both daughter cells through the narrow cytoplasmic bridge connection (Fig. 7A,D) and no mitochondrial fission had occurred, and in others, the two mitochondria were connected via an electron density within the cytoplasmic bridge (Fig. 7B,C, arrow, 7E, insets). This posterior end density could play a role in either mitochondrial fission or attachment of the mitochondrion to the posterior end. Indeed, this density was observed in all G1 stage 1 cells ($n=52$) (Fig. 4E, arrows; 4B, arrows), suggesting a broader role than just fission. Indeed, electron-dense foci were also identified at some of the branch points throughout the mitochondrion (Fig. 7F,G) suggesting a broader role in mitochondrial branching events.

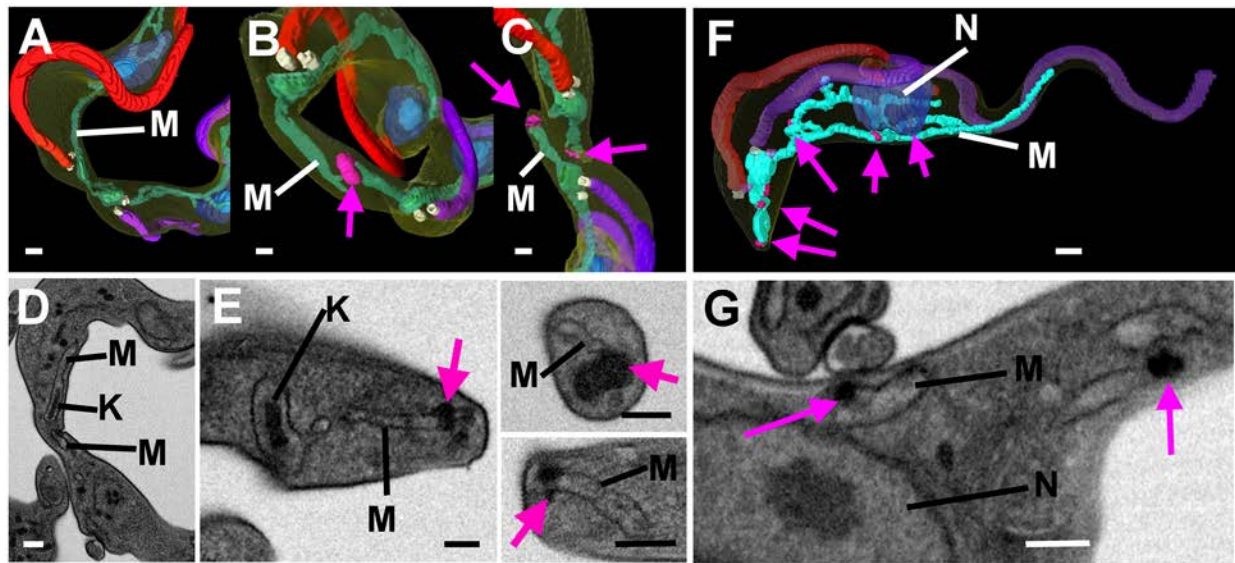


Fig. 7. The mitochondrion is final organelle to separate prior to abscission. (A–C) Surface rendering of segmented stage 8 duplet cells showing the posterior portion of mitochondria (M) that are connected (A,B) and following mitochondrial separation (C), with (B,C) and without the distinctive electron density (pink arrow). (D) SBF-SEM micrograph showing the data modelled in A. The mitochondrion and kinetoplast (K) are indicated. (E) An electron density (pink arrow) is often located at the posterior end of the mitochondrion. (F,G) Surface rendering of segmented data and a micrograph from the same data set showing electron densities associated with the mitochondrion (pink arrows). The nucleus is indicated (N). Scale bars: ~500 nm.

Multiple Golgi bodies are precisely positioned underneath each flagellum during the cell division cycle

In *T. brucei*, the only site for endocytosis and exocytosis is at the flagellar pocket and this restriction is unusual in eukaryotic cells. It is highly active in the mammalian bloodstream form due to the fast turnover of VSG molecules, which are required for immune evasion and represent nearly 10% of all protein made in the cell. Golgi bodies are essential for the biogenesis of VSG and cells must maintain the protective VSG coat as cells increases in size. Golgi bodies were identified easily with clear cisternae (Fig. 4A,B; arrows) and ~4–5 stacks were evident. All Golgi bodies were located beneath a flagellum and closely aligned with the flagellum attachment zone (FAZ) along the long axis of the cell (Fig. 1A,B, Fig. 4A,B,C) as was reported by immunofluorescence microscopy of ER-exit site (ERES) and Golgi body markers (Bangs, 2011). In stage 1 cells, there were either one (60%) or two (40%) Golgi bodies (Fig. 4D). As the cell cycle progressed the number of Golgi bodies increased from three in 70% of stage 3 cells rising to 57% of cells containing at least four Golgi bodies by stage 6 (following mitosis) during formation of the division fold and, in some cells, there were even five or six Golgi bodies during stage 6. However, during furrow ingression in stage 7, the number began to decrease with either three (60%) or two Golgi bodies (40%) being present in stage 8 cells. The increase and decrease across the cell cycle likely reflect the increased requirement for secreted proteins during cell division.

Golgi body positioning along each FAZ was analysed by measuring the distance from the proximal end of the old flagellum to each Golgi body, and this was repeated for Golgi bodies located along the new flagellum. This revealed that Golgi bodies were located at the same relative positions along each flagellum. Golgi bodies closest to the proximal end of both old and new flagella were located 2.6 µm from their respective basal body ($n=36$) (Fig. 4E1). The second and third Golgi (if present) were, on average, located 3.7 µm ($n=26$) and 4.2 µm ($n=7$), respectively, from the basal body (Fig. 4E1; Fig. 8B–D). There was no significant difference between the measurements taken along the old and new

flagellum. In addition, in stage 1 cells with two Golgi, one Golgi was located more posterior to the other beneath the single flagellum, between the flagellar pocket and nucleus (Fig. 1A; Movie 1). However, once the new flagellum had begun to grow, one Golgi body was located with the old flagellum and one with the new flagellum (Fig. 4C; Fig. 8B–D). Taken together, these results demonstrate that even though there are multiple Golgi bodies present throughout the cell cycle, their location was precisely positioned along the FAZ area.

DISCUSSION

In this paper, we have undertaken an in-depth qualitative and quantitative 3D analysis of the how the major mammalian bloodstream form *T. brucei* divides (Fig. 8A). We show that as soon as the new flagellum begins to grow at the start of the cell cycle, the cell body volume increases and all the measured organelles also begin to increase in volume or number, with the exception of acidocalcisomes, which did not increase in number until mitosis. There is positive correlation between cell body volume increase and glycosome number, mitochondrion volume, nucleus volume and cell volume through the cell cycle. Cell volume increase would certainly require an increase in ATP production, which is provided for by an increase in glycosome number. Glycosomes are crucial for the mammalian bloodstream form of this parasite where energy is produced only by glycolysis, and there is a great interest in understanding the pathways involved in ATP production within this organelle (Haanstra et al., 2016). Further work to better understand how these organelles divide and whether this is similar to peroxisome division (Knoblach and Rachubinski, 2016) is now possible by combining SBF-SEM and cellular electron tomography, where glycosome volume could be calculated with greater accuracy and which would allow further dissection of absolute energy requirements for bloodstream form cells.

Regardless of the number or origin of organelles and cell structures, partitioning to each daughter must involve both retention of duplicated organelles and cellular structures by one daughter and

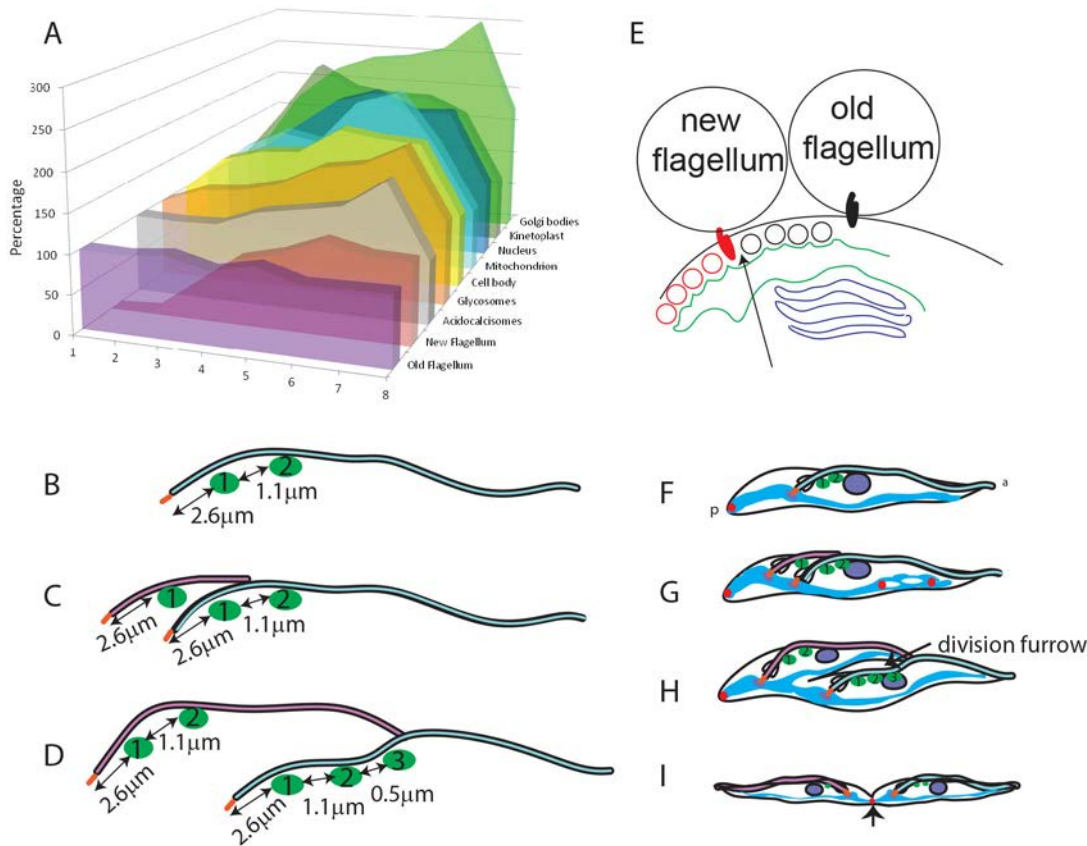


Fig. 8. Summary of key changes through the cell cycle. (A) Chart showing the average percentage changes from G1 cells in volume (cell body, nucleus, kinetoplast, mitochondrion), number (Golgi bodies, glycosomes and acidocalcisomes) and length (old and new flagellum) of each organelle through the cell cycle relative to G1 cells (the length of the new flagellum is relative to the average length of the old flagellum). (B–D) Cartoons illustrating the precise location of Golgi bodies in cells throughout the cell cycle. Single flagellum with two Golgi bodies (B); old flagellum (blue) and new flagellum (pink) (C); in cells later in the cell cycle the precise location is maintained (D). (E) Cartoon illustrating the organization of the FAZ and ER area underneath each flagellum during the early stages of the cell cycle. ER (green) is associated with the old FAZ microtubules (black) and the close proximity of the new FAZ microtubules (red) might be important for location of ER and Golgi body inheritance. (F–I) Cartoon illustrating duplication of Golgi bodies (green) and the mitochondrion with the posterior end electron density and branch densities (red).

delivery to the other daughter. This has been well characterized in *S. cerevisiae* where the cytoskeleton plays a key role in this process (Knoblach and Rachubinski, 2015a). The mechanism of retention and delivery can be clearly seen in *T. brucei* cells through association of organelles with the FAZ area, which ensures that organelles are retained with one daughter and then duplicate to be associated with the other daughter at cell abscission. Organelles and cell structures including basal bodies, the kinetoplast, Golgi bodies, a portion of the ER and nuclei are located along the long axis of the cell closely associated with the seam along the cell body where the flagellum is attached (the FAZ). Although the mitochondrion is located on the ventral side of the cell, opposite the FAZ area, a portion is physically attached to the flagellum at the basal bodies (Ogbadoyi et al., 2003), ensuring inheritance during division. But this does not explain fully how the rest of the mitochondrion is positioned for inheritance to each daughter. We did not model the ER for this analysis, but a portion of the ER is closely associated with the four specialized microtubules of the flagellum attachment zone (FAZ) along the entire length of the flagellum (Lacomble et al., 2012; Vickerman, 1969b), suggesting that they are important for ER inheritance (Fig. 8E). Although no direct linkage has been identified between the nuclear membrane and the FAZ area, the alignment of the nucleus and the positioning of the two lobes during mitosis close to the FAZ area suggest a role in positioning. Glycosomes and acidocalcisomes were located throughout the cell body, suggesting a

more stochastic mechanism for inheritance during furrow ingression. However, this work highlighted that if there is a stochastic mechanism of division of multicopy organelles, the optimal number was quickly established following cytokinesis as each daughter in stage 8 cells already contained a very similar number to stage 1 cells.

Previous immunocytochemistry of ERES proteins showed three, four, five and even six Golgi bodies located along the FAZ area of the flagellum depending on the cell cycle stage (Bangs, 2011; Sevova and Bangs, 2009) and our data supports this work. Either one or two Golgi bodies were present in stage 1 cells, and the difference in Golgi body number in G1 cells could be that a reduction in number does not complete until after cytokinesis, so G1 cells with two Golgi bodies will be those cells that have just recently divided. Alternatively, Golgi body duplication could precede new flagellum growth at the start of the cell cycle and a second Golgi could be formed as the cell prepares for cell volume increases. Our work raises the question of how precise positioning of Golgi bodies is orchestrated (Fig. 8B–D). In *T. brucei*, Golgi body duplication is *de novo*, with formation of a new Golgi from a new ER exit site close to the old Golgi (He et al., 2004; Yelinek et al., 2009). The two Golgi bodies formed within G1 or early in the cell cycle are formed when there is just a single flagellum and FAZ (Fig. 8B). One must segregate with the new flagellum and FAZ, with one remaining with the old flagellum and FAZ (Fig. 8C). The remaining Golgi bodies

form along each flagellum and FAZ at defined positions (Fig. 8D). One possibility is that when microtubules of the new FAZ extend alongside the old FAZ (Wheeler et al., 2013), the ER becomes associated with the new FAZ microtubules, facilitating positional inheritance of both the ER and Golgi bodies (Fig. 8E). Whether there is a specific specialized area for Golgi formation to explain the accurate distance between Golgi bodies or whether other factors, such as the increase in cell size, trigger Golgi formation is yet to be determined, but there must be regulatory factors that control Golgi formation and new flagellum and FAZ growth. In addition, the precise location of Golgi bodies and ERESs raises questions about the dynamic nature of the ER in *T. brucei*. In other eukaryotic cells, the ER is considered a dynamic organelle (Puhka et al., 2012). There is very little research into ER biogenesis in *T. brucei*, but the precise positioning of the Golgi bodies suggests that there could be stable or less-dynamic areas of ER associated with the cytoskeleton.

Using SBF-SEM to provide a 3D view of cells at the ultrastructural level is a major step forward in understanding how multicopy organelles and large undulating organelles are organized and divide in 3D space. We discovered that the mitochondrion was only distributed along the ventral surface, even during branching at mitosis. Further work will be required to understand how this positioning is achieved and whether there are distinct connections to the cytoskeleton to support this (Knobloch and Rachubinski, 2015a; Phillips and Voeltz, 2016). Even though the vast majority of the mitochondrion segregated to the two daughters through stages 6–8, we discovered that the mitochondrion was still connected across the cytoplasmic bridge between the two daughter cells in stage 8, with mitochondrial fission preceding cell abscission. The electron density observed at the posterior end of cells was closely associated with the mitochondrion within the cytoplasmic bridge connection and could contain proteins including dynamin for mitochondrion fission and anchoring the mitochondrion to the posterior end (Fig. 8F–I). Whether the electron-dense structure in the cytoplasmic bridge connection is similar to the midbody, which is involved in abscission in mammalian cells, awaits further investigation (Dionne et al., 2015). The GTPase dynamin was shown to be essential for division of mitochondria in eukaryotic cells (Legesse-Miller et al., 2003; Shpetner and Vallee, 1989), and knockdown of the single dynamin-like protein in *T. brucei* regulates mitochondrial division (Morgan et al., 2004). Further work showed that knockdown led to a precise cell cycle arrest with an accumulation of cells that were still connected at their posterior ends only (Chanez et al., 2006) and thus, were highly similar to the stage 8 cells outlined in this work. We did not observe any fragmentation of the mitochondrion, but branching was observed via expansion into flattened areas and appearance of fenestrations. The frequent electron densities at branch points may suggest a role of GTPases in the formation of fenestrations for branching in addition to constriction sites in mitochondrial fragmentation (Antonny et al., 2016; Legesse-Miller et al., 2003).

Unlike other complex 3D microscopy techniques such as electron tomography, SBF-SEM is a relatively simple technique and will be a valuable tool in many areas of cell biology, enabling biologists to analyse relatively large numbers of whole individual cells at the ultrastructural level. This detailed analysis in *T. brucei* will give a greater understanding of organelle inheritance in these cells and will be important for future studies of many different mutant cell lines. This analysis represents an important step forward in understanding how these cells divide and further analysis of many of the distinctive and novel features outlined in our research will inform many different areas of future trypanosome research.

MATERIALS AND METHODS

T. brucei cultivation and preparation of cells for electron microscopy

T. brucei Lister 427 bloodstream cells were grown in an asynchronous culture in HMI-9 medium (Invitrogen, Paisley, Renfrewshire, UK) supplemented with 15% fetal calf serum (FCS) (Sigma, Gillingham, Dorset, UK) (37°C under 5% CO₂). Cells were harvested at mid-log phase. Fixation was carried out according to the methods in Hughes et al. (2013). In summary, 2.5% glutaraldehyde (TAAB) was applied while the cells were in suspension in the culture medium for 3–5 min. Cells were pelleted and re-suspended in a primary fixative containing 2.5% glutaraldehyde, 2% paraformaldehyde (Agar Scientific) and 0.1% tannic acid (TAAB) in 0.1 M phosphate buffer, pH 7.0 (Sigma), and centrifuged for 3 min. Fresh primary fixative solution was applied to the cell pellet and the cells were fixed for 2 h at room temperature. Pellets were washed with 0.1 M phosphate buffer (pH 7.0) and post-fixed in 1% osmium tetroxide (Agar Scientific) in 0.1 M phosphate buffer (pH 7.0) for 1 h at room temperature. Samples were rinsed and stained *en bloc* for 40 min in 2% aqueous uranyl acetate (TAAB), dehydrated in an ascending acetone series (Fisher Scientific) and embedded in hard formulation Agar 100 resin (Agar Scientific).

SBF-SEM

Resin-embedded samples were trimmed, mounted onto stubs and placed into a Quanta 250FEG (FEI, Eindhoven, Netherlands) with a fitted Gatan 3view system (Gatan, Abingdon, UK). Serial images of the block face were recorded at an accelerating voltage of 5 kV, a spot size of 2.5 and pressure of 0.5 Torr. The dwell time for each micrograph was 5 μ s. Pixel size was 6–6.2 nm and slice thickness was 100 nm (Z-slice) with a horizontal field width of \sim 25 μ m. Up to 1000 slices were collected for each run and five sets of data were collected in total. Images were recorded using Digital Micrograph (Gatan). Images were combined to form a single MRC file format via *etomo* (IMOD, Kremer et al., 1996) which was then smoothed (using clip smooth in 2D) and floated (using newstack float) to ensure even contrast and brightness across the data set (discussed in Starborg et al., 2013). Individual whole cells were selected and boxed out with *etomo* using the trimvol function of IMOD. Raw data is available upon request to the corresponding author.

Data processing and statistical analysis

Segmentation was conducted using AMIRA (versions 5.3.3 to 6.1, FEI, Eindhoven). Whole cells were segmented by selecting a region of interest and applying a threshold based on the density of stain. Manual segmentation of organelles was conducted using the brush tool and was based on ultrastructural characteristics specific to each organelle. Each organelle was segmented using the organelle membrane as the outer edge. Surface models were produced for each segmented organelle. The movies shown in the supplementary material were generated using the demo-maker and movie-maker functions in AMIRA and the 3D measurement tool was used to take measurements. Distance measurements were taken from similar points in 3D space between organelles to enable an accurate comparison across the cell cycle, for example, the most posterior point of the nucleus was always used. When measuring distances between organelles, the most posterior point of each organelle was used as the start and end point of measurement, for example, between the basal bodies and Golgi bodies. Volumes of organelles were automatically generated from the surface renderings of segmented data. The volume of the nuclei included the nucleolus. The volume of the kinetoplast only included the stained DNA region, not the surrounding mitochondrial matrix or membrane. Statistics used were the Student's *t*-test and one way ANOVA.

Acknowledgements

We would like to thank Dr Eva Gluenz, Prof. Gloria Rudenko, Prof. Andre Schneider and members of our laboratories for critical reading of the manuscript and to Prof. Keith Gull for helpful discussion. We also thank the Oxford Brookes Bioimaging Unit.

Competing interests

The authors declare no competing or financial interests.

Funding

This work was funded by the Biotechnology and Biological Sciences Research Council (BB/I000402/1 to S.V., and BB/L014122/1). S.B. was funded by a Nigel Groome Oxford Brookes PhD award.

Supplementary information

Supplementary information available online at <http://jcs.biologists.org/lookup/doi/10.1242/jcs.198887.supplemental>

References

- Antonny, B., Burd, C., De Camilli, P., Chen, E., Daumke, O., Faelber, K., Ford, M., Frolov, V. A., Frost, A., Hinshaw, J. E. et al.** (2016). Membrane fission by dynamin: what we know and what we need to know. *EMBO J.* **35**, 2265-2381.
- Bangs, J. D.** (2011). Replication of the ERES:Golgi junction in bloodstream-form African trypanosomes. *Mol. Microbiol.* **82**, 1433-1443.
- Chanez, A.-L., Hehl, A. B., Engstler, M. and Schneider, A.** (2006). Ablation of the single dynamin of *T. brucei* blocks mitochondrial fission and endocytosis and leads to a precise cytokinesis arrest. *J. Cell Sci.* **119**, 2968-2974.
- Denk, W. and Horstmann, H.** (2004). Serial block-face scanning electron microscopy to reconstruct three-dimensional tissue nanostructure. *PLoS Biol.* **2**, e329.
- Dionne, L. K., Wang, X.-J. and Prekeris, R.** (2015). Midbody: from cellular junk to regulator of cell polarity and cell fate. *Curr. Opin. Cell Biol.* **35**, 51-58.
- Docampo, R. and Huang, G.** (2015). Calcium signaling in trypanosomatid parasites. *Cell Calcium* **57**, 194-202.
- Esseiva, A. C., Chanez, A.-L., Bochud-Allemann, N., Martinou, J.-C., Hemphill, A. and Schneider, A.** (2004). Temporal dissection of Bax-induced events leading to fission of the single mitochondrion in *Trypanosoma brucei*. *EMBO Rep.* **5**, 268-273.
- Farr, H. and Gull, K.** (2009). Functional studies of an evolutionarily conserved, cytochrome b5 domain protein reveal a specific role in axonemal organisation and the general phenomenon of post-division axonemal growth in trypanosomes. *Cell Motil. Cytoskeleton* **66**, 24-35.
- Glunz, E., Povelones, M. L., Englund, P. T. and Gull, K.** (2011). The kinetoplast duplication cycle in *Trypanosoma brucei* is orchestrated by cytoskeleton-mediated cell morphogenesis. *Mol. Cell Biol.* **31**, 1012-1021.
- Haanstra, J. R., González-Marcano, E. B., Gualdrón-López, M. and Michels, P. A. M.** (2016). Biogenesis, maintenance and dynamics of glycosomes in trypanosomatid parasites. *Biochim. Biophys. Acta* **1863**, 1038-1048.
- Hamarton, T. C., Monnerat, S. and Mottram, J. C.** (2007). Cytokinesis in trypanosomatids. *Curr. Opin. Microbiol.* **10**, 520-527.
- He, C. Y.** (2007). Golgi biogenesis in simple eukaryotes. *Cell Microbiol.* **9**, 566-572.
- He, C. Y., Ho, H. H., Malsam, J., Chalouni, C., West, C. M., Ullu, E., Toomre, D. and Warren, G.** (2004). Golgi duplication in *Trypanosoma brucei*. *J. Cell Biol.* **165**, 313-321.
- Hemphill, A., Seebeck, T. and Lawson, D.** (1991). The *Trypanosoma brucei* cytoskeleton: ultrastructure and localization of microtubule-associated and spectrin-like proteins using quick-freeze, deep-etch, immunogold electron microscopy. *J. Struct. Biol.* **107**, 211-220.
- Hughes, L., Towers, K., Starborg, T., Gull, K. and Vaughan, S.** (2013). A cell-body groove housing the new flagellum tip suggests an adaptation of cellular morphogenesis for parasitism in the bloodstream form of *Trypanosoma brucei*. *J. Cell Sci.* **126**, 5748-5757.
- Hughes, L., Hawes, C., Monteith, S. and Vaughan, S.** (2014). Serial block face scanning electron microscopy—the future of cell ultrastructure imaging. *Protoplasma* **251**, 395-401.
- Knoblauch, B. and Rachubinski, R. A.** (2015a). Sharing the cell's bounty - organelle inheritance in yeast. *J. Cell Sci.* **128**, 621-630.
- Knoblauch, B. and Rachubinski, R. A.** (2015b). Transport and retention mechanisms govern lipid droplet inheritance in *Saccharomyces cerevisiae*. *Traffic* **16**, 298-309.
- Knoblauch, B. and Rachubinski, R. A.** (2016). Sharing with your children: mechanisms of peroxisome inheritance. *Biochim. Biophys. Acta* **1863**, 1014-1018.
- Kremer, J. R., Mastrorade, D. N. and McIntosh, J. R.** (1996). Computer visualization of three-dimensional image data using IMOD. *J. Struct. Biol.* **116**, 71-76.
- Lacomble, S., Vaughan, S., Deghelt, M., Moreira-Leite, F. F. and Gull, K.** (2012). A *Trypanosoma brucei* protein required for maintenance of the flagellum attachment zone and flagellar pocket ER domains. *Protist* **163**, 602-615.
- Legesse-Miller, A., Massol, R. H. and Kirchhausen, T.** (2003). Constriction and Dnm1p recruitment are distinct processes in mitochondrial fission. *Mol. Biol. Cell* **14**, 1953-1963.
- Morgan, G. W., Goulding, D. and Field, M. C.** (2004). The single dynamin-like protein of *Trypanosoma brucei* regulates mitochondrial division and is not required for endocytosis. *J. Biol. Chem.* **279**, 10692-10701.
- Ogbadoyi, E. O., Robinson, D. R. and Gull, K.** (2003). A high-order transmembrane structural linkage is responsible for mitochondrial genome positioning and segregation by flagellar basal bodies in trypanosomes. *Mol. Biol. Cell* **14**, 1769-1779.
- Oh, Y. and Bi, E.** (2011). Septin structure and function in yeast and beyond. *Trends Cell Biol.* **21**, 141-148.
- Phillips, M. J. and Voeltz, G. K.** (2016). Structure and function of ER membrane contact sites with other organelles. *Nat. Rev. Mol. Cell Biol.* **17**, 69-82.
- Pollard, T. D. and Wu, J.-Q.** (2010). Understanding cytokinesis: lessons from fission yeast. *Nat. Rev. Mol. Cell Biol.* **11**, 149-155.
- Puhka, M., Joensuu, M., Vihinen, H., Belevich, I. and Jokitalo, E.** (2012). Progressive sheet-to-tubule transformation is a general mechanism for endoplasmic reticulum partitioning in dividing mammalian cells. *Mol. Biol. Cell* **23**, 2424-2432.
- Robinson, D. R., Sherwin, T., Ploubidou, A., Byard, E. H. and Gull, K.** (1995). Microtubule polarity and dynamics in the control of organelle positioning, segregation, and cytokinesis in the trypanosome cell cycle. *J. Cell Biol.* **128**, 1163-1172.
- Sevova, E. S. and Bangs, J. D.** (2009). Streamlined architecture and glycosylphosphatidylinositol-dependent trafficking in the early secretory pathway of African trypanosomes. *Mol. Biol. Cell* **20**, 4739-4750.
- Sherwin, T. and Gull, K.** (1989). The cell division cycle of *Trypanosoma brucei* brucei: timing of event markers and cytoskeletal modulations. *Philos. Trans. R. Soc. Lond. Ser. B Biol. Sci.* **323**, 573-588.
- Shpetner, H. S. and Vallee, R. B.** (1989). Identification of dynamin, a novel mechanochemical enzyme that mediates interactions between microtubules. *Cell* **59**, 421-432.
- Starborg, T., Kalson, N. S., Lu, Y., Mironov, A., Cootes, T. F., Holmes, D. F. and Kadler, K. E.** (2013). Using transmission electron microscopy and 3View to determine collagen fibril size and three-dimensional organization. *Nat. Protoc.* **8**, 1433-1448.
- Tetley, L. and Vickerman, K.** (1991). The glycosomes of trypanosomes: number and distribution as revealed by electron spectroscopic imaging and 3-D reconstruction. *J. Microsc.* **162**, 83-90.
- Tyler, K. M., Matthews, K. R. and Gull, K.** (2001). Anisomorphic cell division by African trypanosomes. *Protist* **152**, 367-378.
- Vaughan, S.** (2010). Assembly of the flagellum and its role in cell morphogenesis in *Trypanosoma brucei*. *Curr. Opin. Microbiol.* **13**, 453-458.
- Vaughan, S. and Gull, K.** (2008). The structural mechanics of cell division in *Trypanosoma brucei*. *Biochem. Soc. Trans.* **36**, 421-424.
- Vercesi, A. E., Moreno, S. N. and Docampo, R.** (1994). Ca²⁺/H⁺ exchange in acidic vacuoles of *Trypanosoma brucei*. *Biochem. J.* **304**, 227-233.
- Verner, Z., Basu, S., Benz, C., Dixit, S., Dobáková, E., Faktorová, D., Hashimi, H., Horáková, E., Huang, Z., Paris, Z. et al.** (2015). Malleable mitochondrion of *Trypanosoma brucei*. *Int. Rev. Cell Mol. Biol.* **315**, 73-151.
- Vickerman, K.** (1969a). The fine structure of *Trypanosoma congolense* in its bloodstream phase. *J. Protozool.* **16**, 54-69.
- Vickerman, K.** (1969b). On the surface coat and flagellar adhesion in trypanosomes. *J. Cell Sci.* **5**, 163-193.
- Vickerman, K. and Preston, T. M.** (1970). Spindle microtubules in the dividing nuclei of trypanosomes. *J. Cell Sci.* **6**, 365-383.
- Wheeler, R. J., Scheumann, N., Wickstead, B., Gull, K. and Vaughan, S.** (2013). Cytokinesis in *Trypanosoma brucei* differs between bloodstream and tsetse trypanostigote forms: implications for microtubule-based morphogenesis and mutant analysis. *Mol. Microbiol.* **90**, 1339-1355.
- Woodward, R. and Gull, K.** (1990). Timing of nuclear and kinetoplast DNA replication and early morphological events in the cell cycle of *Trypanosoma brucei*. *J. Cell Sci.* **95**, 49-57.
- Yelinek, J. T., He, C. Y. and Warren, G.** (2009). Ultrastructural study of Golgi duplication in *Trypanosoma brucei*. *Traffic* **10**, 300-306.